

# Dependence of EC-Driven Current on the EC-Wave Beam Direction in LHD<sup>\*)</sup>

Yasuo YOSHIMURA, Shin KUBO, Takashi SHIMOZUMA, Hiroe IGAMI, Hiromi TAKAHASHI, Masaki NISHIURA, Satoru SAKAKIBARA, Kenji TANAKA, Kazumichi NARIHARA, Takashi MUTOH, Hiroshi YAMADA, Kazunobu NAGASAKI<sup>1)</sup>, Nikolai B. MARUSHCHENKO<sup>2)</sup> and Yuri TURKIN<sup>2)</sup>

*National Institute for Fusion Science, Toki 509-5292, Japan*

<sup>1)</sup>*Institute of Advanced Energy, Kyoto University, Uji 611-0011, Japan*

<sup>2)</sup>*Max-Planck-Institut für Plasmaphysik, EURATOM Association, TI Greifswald, Germany*

(Received 27 December 2010 / Accepted 29 March 2011)

Electron cyclotron current drive (ECCD) experiments were conducted in the Large Helical Device to investigate the characteristics of EC-driven current and its profile and the possibility of controlling current and rotational transform profiles by ECCD. Successful ECCD helps prevent magnetohydrodynamic instabilities in plasmas. Scanning the EC-wave beam direction with a long pulse width of 8 s revealed a systematic change in the plasma current. The current's direction was reversed by a reversal of the beam direction. The direction agrees with the prediction of Fisch–Boozer theory regarding EC-wave beam injection from low-field side. The maximum driven current is 9 kA with an EC-wave power of 100 kW. The optimum beam direction that maximizes the driven current is investigated with the help of ray-tracing code. This direction depends on the magnetic field, efficiency of power absorption, and fraction of the power absorbed by trapped electrons.

© 2011 The Japan Society of Plasma Science and Nuclear Fusion Research

Keywords: ECCD, electron cyclotron current drive, plasma current, LHD, TRAVIS

DOI: 10.1585/pfr.6.2402073

## 1. Introduction

Electron cyclotron current drive (ECCD) is an attractive tool for controlling plasmas. By using a well-focused EC-wave beam, the plasma current can be driven locally so that ECCD can control the plasma current and rotational transform profiles, which affect magnetohydrodynamic (MHD) activity [1-3]. In tokamak-type plasma confinement devices, the effectiveness of ECCD for stabilizing the neoclassical tearing mode, which is a harmful MHD activity, has been demonstrated by driving current within the magnetic island [4-7]. Moreover, ECCD can be suitable for supporting ohmic plasma current startup in tokamaks.

Also, for stellarators that do not need plasma current for plasma confinement, the current profile control capability enables fine plasma control. ECCD can maintain an optimized profile of the rotational transform  $\iota/2\pi$  or locally modify the  $\iota/2\pi$  profile. Eliminating or shifting the rational surfaces suppresses instabilities related to the existence of the surfaces. In the Wendelstein 7-AS stellarator, well-constructed ECCD experiments were conducted and the results were investigated in detail [8]. Moreover, in Heliotron J [9-12] and the Compact Helical System (CHS) [13, 14], ECCD was successfully observed. In the Large

Helical Device (LHD), ECCD was attempted and changes in the plasma current and rotational transform profiles by co- and counter-ECCD were reported [15, 16].

Constraints on the beta value  $\beta$  and its local gradient  $d\beta/d\rho$  at  $\rho = 0.5$  ( $\rho$ : normalized minor radius) because of the onset of magnetic fluctuations caused by the  $m/n = 2/1$  unstable mode ( $m$ : poloidal and  $n$ : toroidal mode numbers) as a dominant component were observed in the LHD [17, 18]. Stabilization of the  $m/n = 2/1$  mode by eliminating the  $\iota/2\pi = 0.5$  surface, resulting in the improvement of  $\beta$  by more than 30%, has been confirmed [17]. The discharges described in Refs. [17] and [18] were performed with a magnetic field of 0.5 T for a high- $\beta$  experiment, and the  $\iota/2\pi = 0.5$  surface was eliminated using a large co-current drive with tangential neutral beam injection. However, controlling the  $\iota$ -profile by ECCD would improve plasma performance and provide experimental flexibility in discharges with higher magnetic fields.

This study describes the results of a recent ECCD experiment in the LHD and emphasizes the dependence of the plasma current on the EC-wave beam injection angle for ECCD. The LHD and the system for the ECCD experiment are briefly described in Sec. 2. Section 3 describes an observation of plasma current in an EC-wave beam injection angle scan experiment. In Sec. 4, the experimental data are compared with results calculated us-

author's e-mail: yoshimura.yasuo@lhd.nifs.ac.jp

<sup>\*)</sup> This article is based on the presentation at the 20th International Toki Conference (ITC20).

ing the TRAVIS code [19], which was originally developed for the investigation of electron cyclotron heating (ECH)/ECCD/electron cyclotron emission (ECE) at Wendelstein 7-X. The study is summarized in Sec. 5.

## 2. LHD and ECCD System

The LHD is a helical device with a toroidal period number  $m = 10$  and a polarity of  $l = 2$ . A magnetic field structure with a rotational transform for plasma confinement is generated entirely by external superconducting coils such as two helical coils and three pairs of poloidal coils [20]. The major radius, or the position of the magnetic axis  $R_{ax}$  of the LHD plasma, can be varied in the range 3.42–4.1 m. The average plasma minor radius is  $\sim 0.6$  m, and the maximum magnetic field at the magnetic axis is  $\sim 3$  T. These values and the characteristics of the magnetic field structure, such as rotational transform profile and magnetic field along the magnetic axis, depend on  $R_{ax}$ .

The magnetic field distributions along the magnetic axis for three  $R_{ax}$  cases are plotted in Fig. 1 as functions of toroidal angle. At  $R_{ax} = 3.75$  m, the magnetic field on the magnetic axis is nearly constant whereas at  $R_{ax} = 3.6$  or 3.9 m, magnetic ripples of  $\sim 5\%$  exist. The ECCD experiments described in this study were performed with a magnetic configuration of  $R_{ax} = 3.75$  m to minimize the effect of magnetic ripples, that is, mirror-trapping effect on ECCD. The magnetic field on the axis is  $\sim 1.5$  T, which is the second harmonic resonance field for a frequency of 84 GHz.

The EC-wave beam injection systems on the LHD provide a two-dimensionally steerable mirror that enables beam direction control. One of the beam injection systems used for the ECCD experiment consists of two inner-vessel

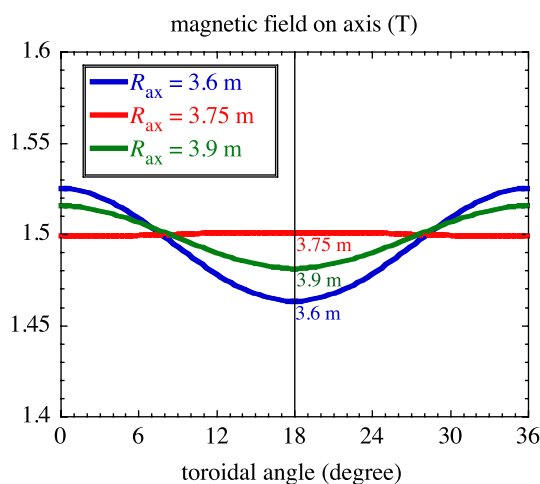


Fig. 1 Magnetic field distributions along magnetic axis for magnetic axis positions  $R_{ax} = 3.6$ , 3.75, and 3.9 m. At  $R_{ax} = 3.75$  m, magnetic ripples are negligible, minimizing the trapping effect for electrons near the magnetic axis.

mirrors. One of the mirrors transforms the EC wave, which is radiated from a waveguide inserted in the LHD vacuum vessel, to a focused circular Gaussian beam. The other plane mirror is used to change the beam direction. The beam waist of the focused beam has a radius ( $1/e$  radius of the electric field amplitude) of 30 mm on the equatorial plane. The injection system is installed at the bottom port of the LHD (1.5-L port), and the beam is injected from the low magnetic field side (LFS). The toroidal angle at the 1.5-L port is defined as 0 (or 36) degrees.

## 3. Results of ECCD Experiment

### 3.1 Time evolution of plasma current in LHD

The EC-wave beam direction should be toroidally tilted for ECCD. Figure 2 shows a schematic representation that illustrates the experimental configuration, EC-wave beam direction  $N_{//}$ , and plasma current direction.  $N_{//}$  is defined as the cosine of the angle between the beam unit vector and the tangent of the magnetic axis at the cross point of the beam and the magnetic axis. According to the Fisch–Boozer theory [21], an EC-wave beam injected from the LFS with positive (negative)  $N_{//}$  couples primarily with electrons moving in the negative (positive)  $I_p$  direction, thus the wave is expected to generate an EC-driven current in the positive (negative)  $I_p$  direction.

Figure 3 shows an example of discharge waveforms in the ECCD experiment. The plasma was generated at 1 s with 82.7 (220 kW, 300 ms) and 84 GHz (100 kW) EC

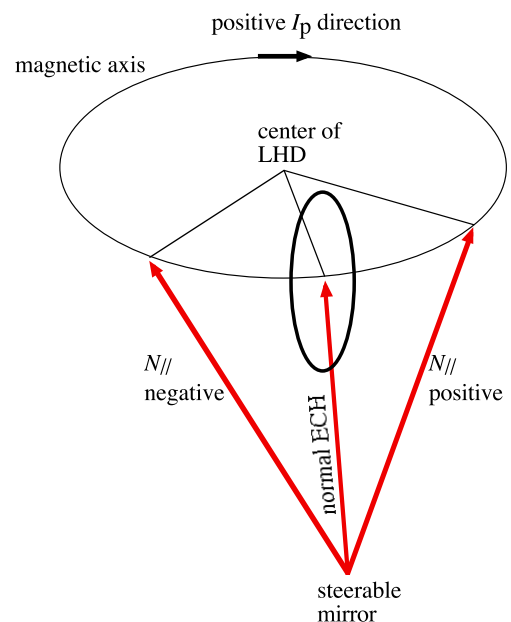


Fig. 2 Schematic representation of the experimental configuration of EC-wave beam injection showing the direction of  $N_{//}$  and plasma current  $I_p$ .  $N_{//}$  is defined as the cosine of the angle between the beam unit vector and the tangent of the magnetic axis at the cross point of the beam and the magnetic axis.

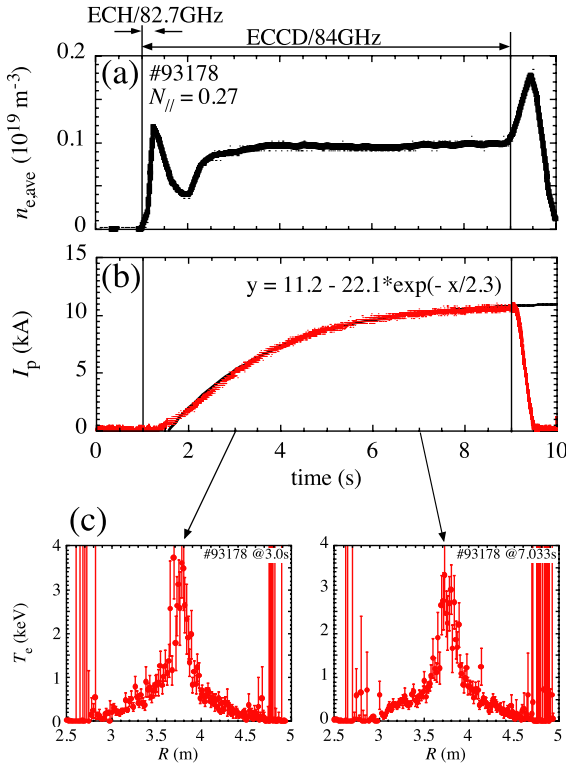


Fig. 3 Example of time evolution of the line-average electron density (a), plasma current (b) and electron temperature profiles at 3 and 7 s (c) for positive ECCD ( $N_{||} = 0.27$ ). Density was kept constant at  $0.1 \times 10^{19} \text{ m}^{-3}$ , and temperature profile was kept nearly constant; current requires  $\sim 6$  s to reach saturation. An exponentially saturating curve with a time constant of 2.3 s fits the current evolution well.

waves; it was sustained by the 84-GHz wave for 8 s. The 84-GHz wave was obliquely injected and aimed at the magnetic axis with  $N_{||}$  of 0.27 and with right-hand circular polarization, which is close to the X mode in the case of oblique injection. The power absorption efficiency of a pure X-mode wave was calculated to be  $\sim 90\%$  using the experimentally obtained plasma parameters and their profiles. On the other hand, that of an O-mode wave is  $\sim 6\%$ . We confirmed that plasmas could not be sustained effectively by an obliquely injected EC-wave beam with left-hand circular polarization (nearly O-mode).

Except for an initial variation, the line-average electron density,  $n_{e,ave}$ , was kept nearly constant at  $0.1 \times 10^{19} \text{ m}^{-3}$  for 6.5 s until the end of the discharge [Fig. 3 (a)]. The electron temperature,  $T_e$ , and its peaked profile were also kept constant with a central electron temperature  $T_{e0}$  of  $\sim 3.5$  keV [Fig. 3 (c)]. On the contrary, the plasma current,  $I_p$ , continued to increase during the discharge. An exponentially saturating fitting curve is also plotted with the time evolution of  $I_p$  in Fig. 3 (b); from the fitting, the time constant of the current saturation is evaluated to be 2.3 s. Here,  $n_{e,ave}$ ,  $T_e$ , and  $I_p$  are measured with a far-infrared interferometer, Thomson scattering measurement system, and Rogowski coil surrounding the plasma, respectively.

Applying a simple  $L/R$  model ( $L$ : plasma inductance,  $R$ : plasma resistance) to the plasma using a volume-average  $T_e$  of 0.4 keV, the time constant is estimated to be 4.3 s. Although a discrepancy exists between the time constants obtained experimentally and with the  $L/R$  model, the time constant is in the range of a few seconds or more. Thus, for reliable measurement of the EC-driven current, long-pulse discharges are necessary.

### 3.2 Dependence of plasma current on EC-wave beam direction

An  $N_{||}$ -scan experiment was performed to optimize the ECCD. The magnetic configuration was  $R_{ax} = 3.75$  m with  $B_{ax} = 1.477$  T.  $B_{ax}$  was slightly reduced from the second harmonic resonant field of the 84-GHz wave, 1.5 T, to consider the Doppler effect. For example, at  $N_{||} = 0.27$ , electrons having a parallel energy,  $m_e v_{||}^2/2$ , of 0.77 keV satisfy the second harmonic Doppler-shifted resonance condition  $2\omega_c = \omega - k_{||}v_{||}$  on the magnetic axis. Here,  $m_e$ ,  $v_{||}$ ,  $\omega_c$ ,  $\omega$ ,  $k_{||}$  denote the electron mass, electron velocity parallel to the magnetic field, angular electron cyclotron frequency, angular frequency of the heating wave, and wave number parallel to the magnetic field, respectively.

The EC-wave beam direction was toroidally scanned while maintaining the beam's aiming position on the magnetic axis. Plasmas were generated and sustained as described in Sec. 3.1. for Fig. 3. The wave polarization was right-hand circular for non-zero  $N_{||}$ . The electron density was kept rather low at around  $0.1 \times 10^{19} \text{ m}^{-3}$ . The dependence of the plasma current  $I_p$  at 9 and 2.5 s on  $N_{||}$  is plotted in Fig. 4. The lack of  $I_p$  data at 9 s means that the discharge could not be sustained for 8 s.  $I_p$  changes direction according to the change in the sign of  $N_{||}$ , and the direction of  $I_p$  agrees with that predicted by Fisch–Boozer theory. At  $N_{||}$  values of 0.27 and  $-0.29$ ,  $I_p$  shows positive and negative maxima, respectively. Simply assuming the bootstrap currents  $I_{BS}$  of the plasmas with various  $N_{||}$  to be equal, and  $I_{BS} = \sim 1$  kA considering  $I_p$  values at large  $|N_{||}|$ , the maximum driven current  $I_{ECCD}$  in the positive  $I_p$  direction is estimated to be  $\sim 9$  kA, and the maximum  $I_{ECCD}$  in the negative  $I_p$  direction is  $\sim -5$  kA. A positive and low  $I_{BS}$  with  $R_{ax} = 3.75$  m in the low- $\beta$  plasma is consistent with a theoretical prediction [22]. Using the maximum  $I_{ECCD}$  of 9 kA with  $T_{e0}$  of 3.5 keV, the current drive efficiency,  $\gamma = n_e R_{ax} I_{ECCD} / P_{abs}$ , and a nondimensional current drive efficiency [23] that includes the contribution of electron temperature,  $\zeta = e^3 n_e R_{ax} I_{ECCD} / (\epsilon_0^2 P_{abs} T_e)$ , are evaluated to be  $3.9 \times 10^{17} \text{ AW}^{-1} \text{ m}^{-2}$  and 0.036, respectively. Here,  $n_e$ ,  $P_{abs}$ ,  $e$ ,  $\epsilon_0$ , and  $T_e$  are the electron density, absorbed EC-wave power, unit charge, permittivity of free space, and electron temperature (electron energy in units of C\*V here), respectively.

For  $N_{||} = 0$ , that is, for normal injection (ECH), the polarization was set to the linear X mode. However, for  $N_{||} = \sim 0$ , plasmas could not be sustained owing to poor one-path absorption at this magnetic field.

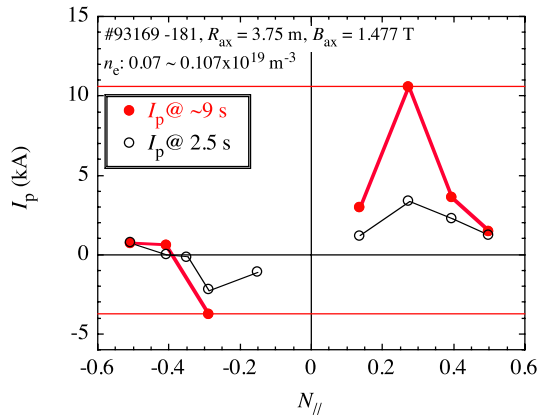


Fig. 4 Dependence of plasma current  $I_p$  on EC-wave beam direction  $N_{||}$ .  $I_p$  shows positive and negative peaks against variations in  $N_{||}$ .

#### 4. Comparison with TRAVIS Code Calculation

The ray-tracing code TRAVIS can calculate the EC-wave absorption and EC-driven current  $I_{\text{ECCD}}$  by using a practical 3D magnetic field configuration and the properties of the plasmas and EC waves [19]. It was originally developed for ECH/ECCD/ECE studies in the Wendelstein 7-X stellarator. It can also be applied to the LHD by using the LHD magnetic field configuration data file. The experimentally obtained dependence of the plasma current on the EC-wave beam direction described in Sec. 3 is compared with that calculated using TRAVIS. In Fig. 5, the calculated  $I_{\text{ECCD}}$  and the power absorption efficiency  $\eta_{\text{abs}}$  for  $B_{\text{ax}} = 1.477$  T are plotted as functions of the EC-wave beam direction  $N_{||}$ . The dependence of  $I_p$  on  $N_{||}$  obtained in the ECCD experiment is well reproduced by the calculation except for the absolute value of  $I_{\text{ECCD}}$ . The calculated  $I_{\text{ECCD}}$  shows positive and negative peaks with an optimum  $N_{||}$  ( $N_{||,\text{opt}}$ ) of  $\sim \pm 0.28$ , and  $\eta_{\text{abs}}$  shows poor power absorption with  $N_{||}$  around 0. Thus, for  $|N_{||}| < |N_{||,\text{opt}}|$ , the decrease in  $|I_{\text{ECCD}}|$  results from the poor power absorption. On the other hand, the calculation shows that the decrease in  $|I_{\text{ECCD}}|$  for  $|N_{||}| > |N_{||,\text{opt}}|$  results from an increase in the fraction of EC-wave power absorbed by the electrons trapped in magnetic ripples. The tendency is like this: the fraction of power absorbed by the trapped electrons over total absorbed power is less than 6% for  $|N_{||}| < |N_{||,\text{opt}}|$ , whereas that for  $|N_{||}| > |N_{||,\text{opt}}|$  increases to more than 30%.

One reason for the discrepancy between the absolute value of the driven current calculated with TRAVIS and that obtained experimentally would be the imperfect settings of the polarization as a pure X mode and the beam direction in the experiment.

The TRAVIS calculation with a  $B_{\text{ax}}$  value of just the second harmonic resonance condition, 1.5 T, was also performed. The result was compared with that of the  $N_{||}$  scan experiment performed with  $B_{\text{ax}} = 1.5$  T. The experiment

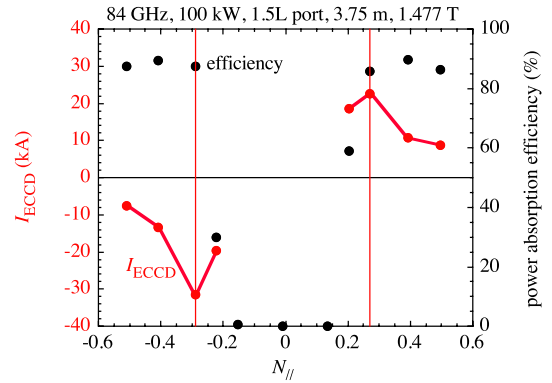


Fig. 5 EC-driven current  $I_{\text{ECCD}}$  and power absorption efficiency calculated with TRAVIS code for  $B_{\text{ax}} = 1.477$  T as functions of the EC-wave beam direction  $N_{||}$ .

was performed with an EC-wave pulse width of 600 ms. With this pulse width, the plasma current was still increasing and was not saturated. However,  $I_p$  at 600 ms is nearly proportional to the saturated  $I_p$  with a sufficiently long pulse discharge. The experimentally obtained  $|N_{||,\text{opt}}|$  was  $\sim 0.2$ , smaller than that in the case of  $B_{\text{ax}} = 1.477$  T. Similar to the experimental result, the calculated  $|N_{||,\text{opt}}|$  also decreased to  $\sim 0.15$ . Owing to the increase in the magnetic field to 1.5 T, the  $N_{||}$  region of poor power absorption became narrower. The absorption is poor even in the case of  $B_{\text{ax}} = 1.5$  T, because the EC-wave beam path with  $N_{||} \sim 0$  is nearly tangential to the plane of  $B = 1.5$  T. Thus, half of the beam passes by the resonance layer when the beam center is aimed at the magnetic axis. Beam refraction also degrades the power absorption.

The TRAVIS calculation with  $B_{\text{ax}} = 1.51$  T reveals that the power absorption was sufficient for any  $N_{||}$ ; in particular, for  $|N_{||}| < 0.3$ , it was larger than 95%. The value of  $|N_{||,\text{opt}}|$  shifted to  $\sim 0.1$ . The decrease in  $|I_{\text{ECCD}}|$  for  $|N_{||}| < |N_{||,\text{opt}}|$  results from insufficient  $N_{||}$  to generate EC-driven current.

Considering the experimental and calculated results with various  $B_{\text{ax}}$  settings of 1.477, 1.5, and 1.51 T described above, the value of  $|N_{||,\text{opt}}|$  is determined by factors such as the power absorption related to the  $B_{\text{ax}}$  setting and the ECCD efficiency related to the  $N_{||}$  setting.

#### 5. Conclusions

An ECCD experiment performed in the LHD was described and the time evolution of the EC-driven current and the dependence of the driven current on the EC-wave beam direction were emphasized. In the LHD, the current diffusion time is typically longer than a few seconds. To measure the fully saturated driven current, EC waves of 84 GHz and 100 kW with an 8-s pulse width were applied in the second harmonic resonance condition. By scanning the EC-wave beam direction for ECCD, the optimum beam directions that maximize the driven current in the posi-

tive and negative current directions were identified. With the optimum beam direction, the maximum driven current reached 9 kA.

The dependence of the EC-driven current on the EC-wave beam direction calculated with the TRAVIS code well reproduced the experimentally obtained dependence, except for the absolute value of the driven current. The optimum beam direction that maximizes the EC-driven current depends on the magnetic field, efficiency of power absorption, and fraction of the power absorbed by trapped electrons.

## Acknowledgments

The authors thank the NIFS staff for performing the LHD experiments. This work was conducted under the framework of a bidirectional collaborative research program between Kyoto University and the National Institute for Fusion Science (KOAR010, KLRR304). This work was partly supported by KAKENHI (Grant-in-Aid for Scientific Research (C), 21560862).

- [1] V. Erckmann and U. Gasparino, *Plasma Phys. Control. Fusion* **36**, 1869 (1994).
- [2] B. Lloyd, *Plasma Phys. Control. Fusion* **40**, A119 (1998).
- [3] R. Prater, *Phys. Plasmas* **11**, 2349 (2004).
- [4] H. Zohm *et al.*, *Nucl. Fusion* **39**, 577 (1999).
- [5] R. Prater *et al.*, *Nucl. Fusion* **47**, 371 (2007).
- [6] A.C.C. Sips *et al.*, *Nucl. Fusion* **47**, 1485 (2007).
- [7] A. Isayama *et al.*, *Nucl. Fusion* **49**, 055006 (2009).
- [8] H. Maassberg *et al.*, *Plasma Phys. Control. Fusion* **47**, 1137 (2005).
- [9] G. Motojima *et al.*, *Nucl. Fusion* **47**, 1045 (2007).
- [10] K. Nagasaki *et al.*, *Plasma Fusion Res.* **3**, S1008 (2008).
- [11] K. Nagasaki *et al.*, *Nucl. Fusion* **50**, 025003 (2010).
- [12] K. Nagasaki *et al.*, *Proc. 23rd IAEA Fusion Energy Conference (2010) EXW/P7-19*.
- [13] Y. Yoshimura *et al.*, *Journal of Korean Physical Society* **49**, S197 (2006).
- [14] Y. Yoshimura *et al.*, *Fusion Sci. Technol.* **53**, 54 (2008).
- [15] T. Notake *et al.*, *Plasma Fusion Res.* **3**, S1077 (2008).
- [16] Y. Yoshimura *et al.*, *Fusion Sci. Technol.* **58**, 551 (2010).
- [17] S. Sakakibara *et al.*, *Plasma Fusion Res.* **1**, 003 (2006).
- [18] K.Y. Watanabe *et al.*, *Fusion Sci. Technol.* **46**, 24 (2004).
- [19] N.B. Marushchenko *et al.*, *Nucl. Fusion* **48**, 054002 (2008); Marushchenko *et al.*, *Nucl. Fusion* **49**, 129801 (2009).
- [20] O. Motojima *et al.*, *Phys. Plasmas* **6**, 1843 (1999).
- [21] N.J. Fisch and A.H. Boozer, *Phys. Rev. Lett.* **45**, 720 (1980).
- [22] K.Y. Watanabe *et al.*, *Nucl. Fusion* **41**, 63 (2001).
- [23] T.C. Luce *et al.*, *Phys. Rev. Lett.* **83**, 4550 (1999).